

Multicolor miRNA fluorescence in situ hybridization for tumor differential diagnosis

Neil Renwick^{1†}, Pavol Cekan^{1†}, Paul A. Masry², Sean E. McGeary¹, Jason B. Miller¹, Markus Hafner¹, Zhen Li¹, Aleksandra Mihailovic¹, Pavel Morozov¹, Miguel Brown¹, Tasos Gogakos¹, Mehrpouya B. Mobin¹, Einar L. Snorrason¹, Harriet E. Feilotter², Xiao Zhang², Clifford S. Perlis³, Hong Wu³, Mayte Suarez-Farinas⁴, Huichen Feng⁵, Masahiro Shuda⁵, Patrick S. Moore⁵, Victor A. Tron², Yuan Chang⁵, Thomas Tuschl¹

AFFILIATIONS

¹Howard Hughes Medical Institute, Laboratory of RNA Molecular Biology, The Rockefeller University, New York, NY 10065; ²Department of Pathology and Molecular Medicine, Queen's University, Ontario, Canada; ³Departments of Surgery and Pathology, Fox Chase Cancer Center, Philadelphia, PA 19111; ⁴Rockefeller University Center for Clinical and Translational Science_Biostatistics, New York, NY 10065; ⁵Cancer Virology Laboratory, University of Pittsburgh Cancer Institute, Pittsburgh, PA 15213; [†]These authors contributed equally to the manuscript.

CORRESPONDING AUTHOR

Prof. Thomas Tuschl, HHMI_Laboratory of RNA Molecular Biology, The Rockefeller University, Box 186 New York, NY 10065; email: ttuschl@rockefeller.edu, tel: +1 212 327 7651, fax: +1 212 327 7652

TABLE OF CONTENTS

Fig. S1. Total miRNA concentrations in clinical samples.....	4
Fig. S2. miR-205 and miR-375 concentrations in clinical samples.....	5
Fig. S3. RNA elution and retention during miRNA FISH.....	6
Fig. S4. Mechanism of EDC crosslinking of 5' phosphorylated RNA and protein in 1-methylimidazole... 7	
Fig. S5. EDC-mediated condensation using adenosine 5' monophosphate and a lysine-reactive peptide to model EDC crosslinking between a 5' phosphate RNA and protein.....	8
Fig. S6. Specificity of EDC-mediated condensation reaction.	9
Fig. S7. Schematic diagram of ABINA synthesis.....	10
Fig. S8. Carbodiimide-mediated condensation using UV-absorbing model compounds.....	11
Fig. S9. EDC-based condensation of ABINA and PAA indicating EDC-based crosslinking between proteins.....	12
Fig. S10. EDC-based retention of long (rRNA) and short (miRNA) RNAs in FFPE tissues.	13
Fig. S11. Increased linker length between oligonucleotide and hapten enables the use of signal amplification systems without tissue permeabilization.....	14
Fig. S12. miR-375 LNA-probe design.....	15
Fig. S13. miR-205 LNA-probe design.....	16
Fig. S14. Workflow diagram of optimized miRNA FISH protocol.....	17
Fig. S15. miRNA signal normalization and establishment of cut-off values for tumor differentiation.....	18
Fig. S16. Confirmation of miR-205 probe specificity in mouse skin tissues.	19
Fig. S17. Confirmation of miR-375 probe specificity in mouse pancreas tissues.....	20
Fig. S18. EDC fixation is incompatible with immunohistochemical staining.	21

Table S1. Total RNA isolation from clinical samples.	22
Table S2. Small RNA sequence read counts and annotation.....	23
Table S3. Total and specific miRNA concentrations in clinical samples.....	24
Table S4. Optimized condensation reaction conditions using different carbodiimide derivatives.	25
Table S5. Optimized condensation reaction conditions using different heterocyclic derivatives and EDC-HCl.....	26
Table S6. miRNA and rRNA probe sequences and melting temperatures of duplexes with target RNA.....	27
Table S7. miRNA signal normalization and establishment of cut-off values to enable tumor differential diagnosis.....	28
Table S8. Fluorescent dyes and their properties, and filters for fluorescent imaging.....	29

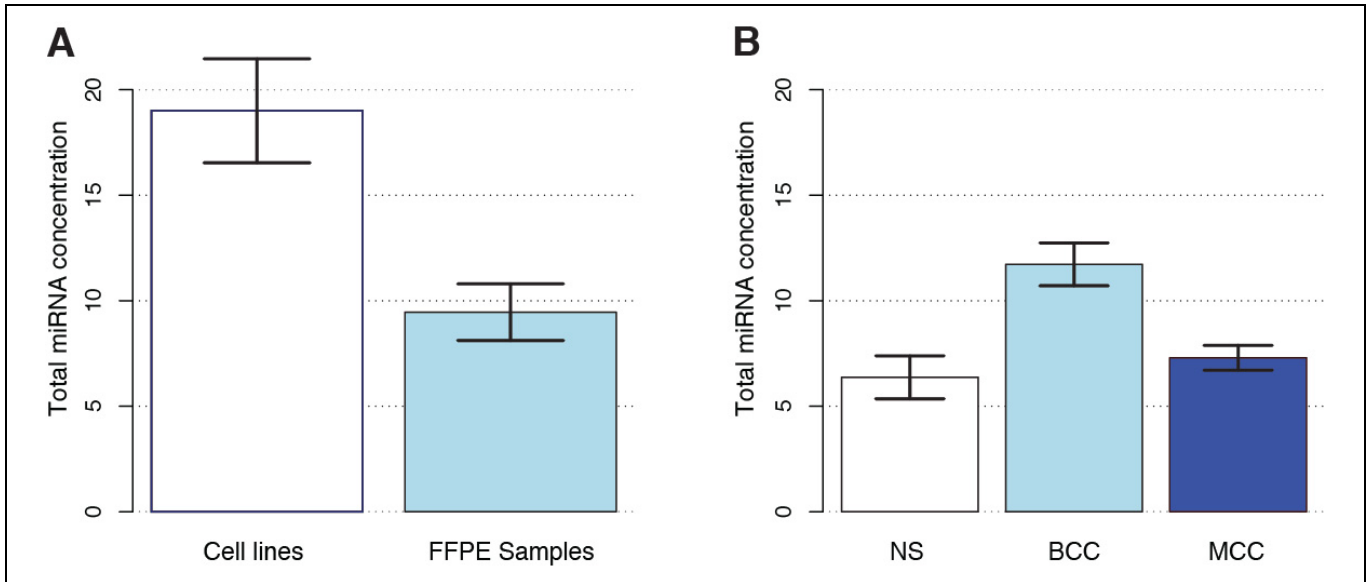


Fig. S1. Total miRNA concentrations in clinical samples. (A) Mean total miRNA concentrations (fmol/μg total RNA) were higher for cell lines than for archived FFPE materials (ANOVA $p < 0.001$, $N_{CL}=8$, $N_{FFPE}=27$). (B) Significant differences in mean total miRNA concentrations were seen between groups (ANOVA $p < 0.001$, $N_{MCC}=12$, $N_{BCC}=4$, $N_{NS}=4$); mean total miRNA concentrations were respectively 4.43 ($p_{adj}=0.004$) and 5.35 ($p_{adj}=0.005$) fmol/μg total RNA higher in BCC than in MCC or NS whereas no significant difference was seen between MCC and NS ($p_{adj}=0.72$). Error bars indicate the standard error of the mean.

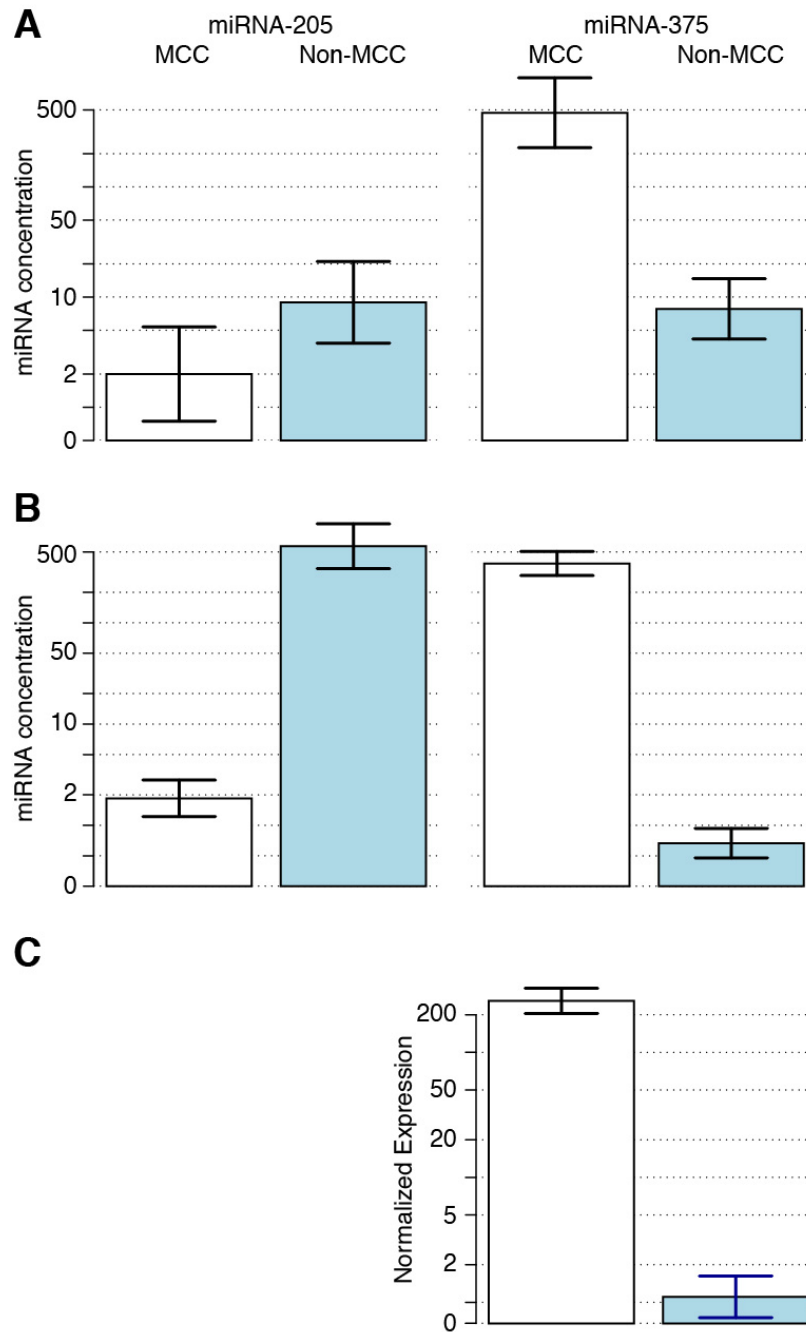


Fig. S2. miR-205 and miR-375 concentrations in clinical samples. Sequencing-derived miR-205 and miR-375 concentrations (fmol/ μ g total RNA) are depicted for **(A)** all samples and **(B)** training set samples. miRNA microarray and real-time RT-PCR analyses of a subset of six MCC and two NS samples confirmed our sequencing-based results. Principal component analysis differentiated MCC from non-MCC (NS) groups (data not shown). miR-205 was 505-fold higher in NS than MCC ($p=0.003$) and miR-375 was 310-fold higher in MCC than NS ($p=0.006$). miR-375 real-time RT-PCR expression levels were assessed for **(C)** 11 MCC and 4 NS samples and were significantly higher in MCC compared to NS (ANOVA $p<0.001$, $N_{\text{MCC}}=11$, $N_{\text{NS}}=4$, $F_{\text{CH}}=233.5$). miR-205 expression was not assessed due to paucity of material. Sequencing-derived miR-375 concentrations and real-time PCR measurements correlated strongly (Spearman correlation 0.94 ($p<0.001$)); Pearson correlation of log₂-transformed variables 0.99 ($p<0.001$). Error bars indicate the standard error of the mean.

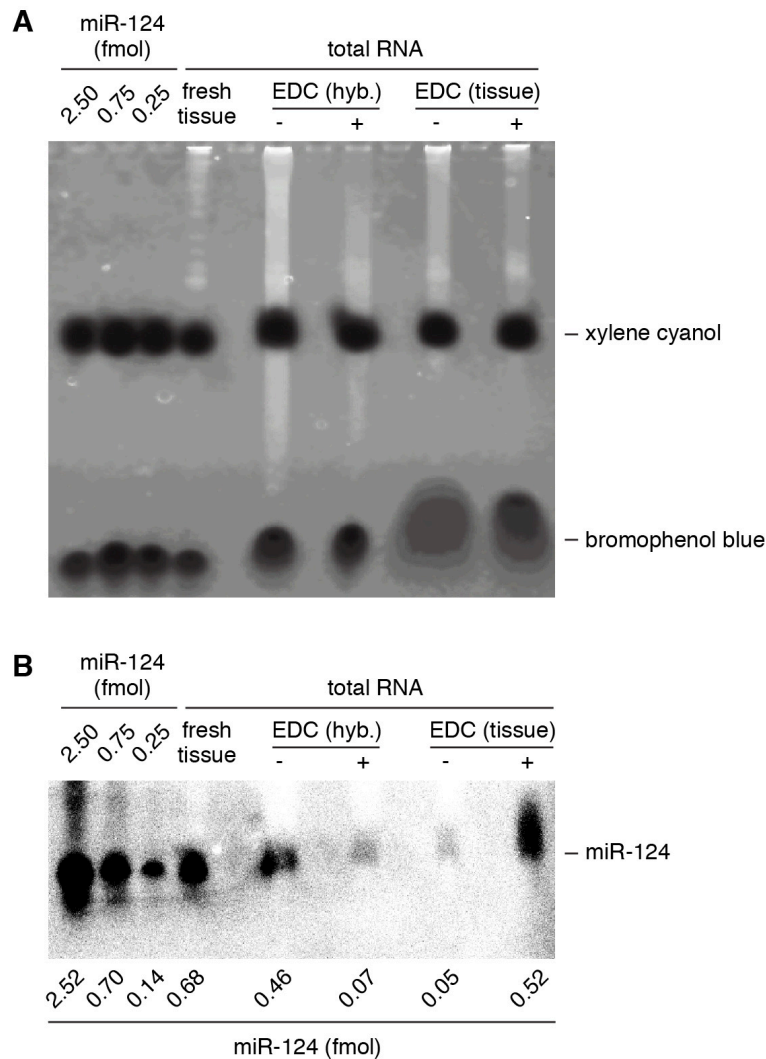


Fig. S3. RNA elution and retention during miRNA FISH. (A) 150 mg of 10 μ m slices of FFPE monkey brain tissue were deparaffinized, rehydrated, refixed with 4% PFA, and processed with (+EDC) and without (-EDC) EDC fixation; 50% total tissue weight was attributed to paraffin. To monitor the loss of RNA during probe hybridization, tissue slices were then incubated for 16 h at 50 $^{\circ}$ C in hybridization solution (hyb) and total RNA was recovered from hyb and incubated tissue. We respectively recovered 115 μ g total RNA (83 μ g hyb. and 32 μ g tissue) but only 31 μ g total RNA (16 μ g hyb. and 15 μ g tissue) from -EDC and +EDC samples as determined by UV 260 nm absorbance. From 100 mg fresh tissue, we obtained 140 μ g of total RNA. The amount of total RNA recovered from +EDC tissue is likely underestimated; RNA enmeshed in irreversibly EDC-crosslinked protein presumably distributed to the phenol/chloroform phase during the RNA isolation. Half of each RNA sample was separated on a 15% polyacrylamide gel and visualized through ethidium bromide staining prior to Northern blotting. (B) Quantitative Northern blot analysis was used to determine miR-124 content in -EDC and +EDC hyb. buffers and tissues. Based on signal intensities for defined amounts of synthetic miR-124, we found that 0.46 and 0.05 fmol miR-124 was respectively lost and retained in -EDC hyb and tissue whereas 0.07 and 0.52 fmol miR-124 was respectively lost and retained in +EDC hyb and tissue. The total amount of miR-124 recovered from hyb and tissue was comparable for -EDC and +EDC samples. The signal of miR-124 from 4 μ g of total RNA from fresh tissue corresponded to 0.68 fmol, therefore indicating that approx. 90% miR-124 present in fresh tissue escaped prior to hybridization. Two other replicates of these experiments showed losses of miR-124 of 50-70%. The escape of miR-124 likely occurred during deparaffinization and rehydration steps and refreshing of formalin-fixation of tissue slices prior to EDC-fixation. In summary, EDC fixation resulted in at least 10-fold better retention of miRNAs and 5-times better retention of longer RNAs during probe hybridization.

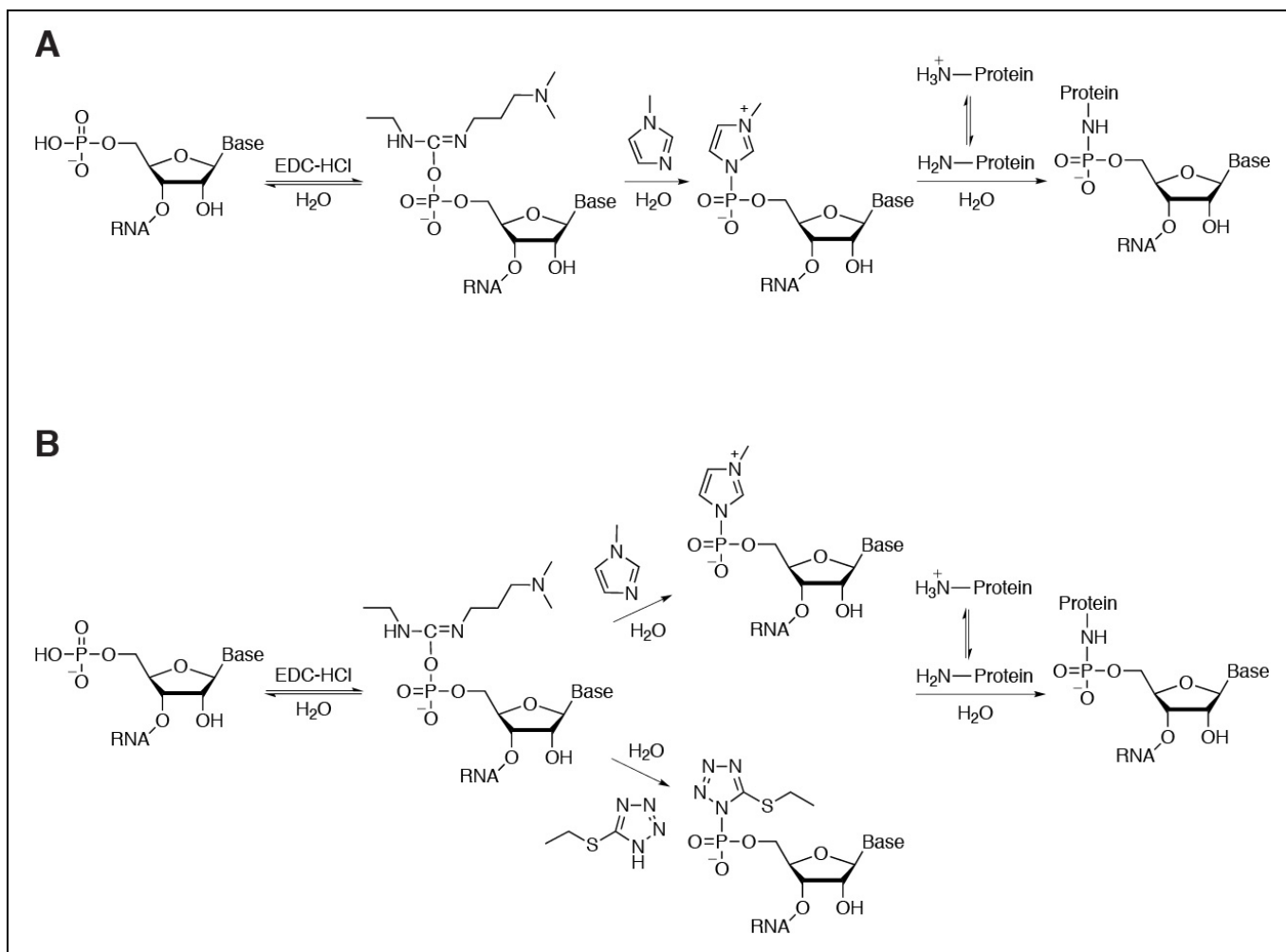


Fig. S4. Mechanism of EDC crosslinking of 5' phosphorylated RNA and protein in 1-methylimidazole. (A) EDC activation of the 5'-phosphate group is the first step of the crosslinking reaction. Due to the short half-life of EDC-activated miRNA in water, 1-methylimidazole was used to form a more stable reaction intermediate, reacting with an amino group on the peptide to form a stable phosphoamide bond; the formation of EDC-activated miRNA and 1-methylimidazole-miRNA intermediates were confirmed by HPLC (data not shown). When 1-methylimidazole was replaced with triethylamine, MOPS, or HEPES buffers (lacking phosphate and primary amines), the crosslinking reaction time increased considerably (> 30-fold) indicating the participation of 1-methylimidazole in EDC crosslinking. The EDC crosslinking reaction is affected by hydrolysis of EDC adducts that can be reduced by reacting with heterocyclic derivatives. Protonation of amines also affects the EDC crosslinking reaction; it would be preferable to carry out the reaction at basic pH, given the pKa of 10.5 for the Lys side chain, however, hydroxide ions begin to compete for the nucleophilic attack of the EDC-5'-p-RNA intermediate under these conditions. Therefore, the reaction was performed at pH 8 to balance the effects of side reactions for optimal EDC crosslinking. (B) Addition of 5-ETT decreased the reaction time for EDC crosslinking through competing intermediate formation.

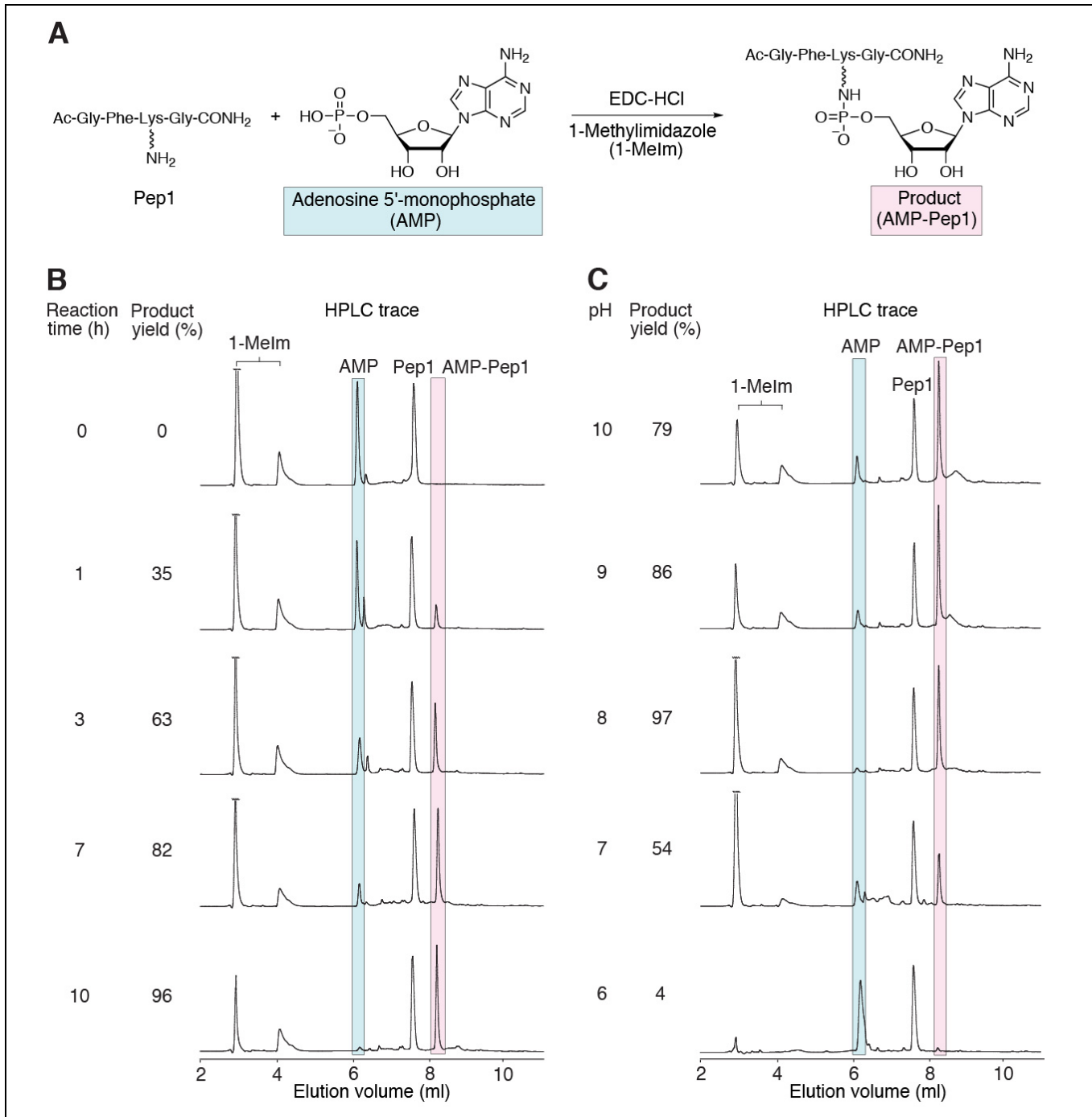


Fig. S5. EDC-mediated condensation using adenosine 5' monophosphate and a lysine-reactive peptide to model EDC crosslinking between a 5' phosphate RNA and protein. (A) The reaction between AMP and peptide Pep1 (Phe was included in the peptide to allow for monitoring of the peptide by UV) at 50 °C, yielded a stable phosphoramidate product AMP-Pep1. AMP was reacted with an excess of Pep1 and EDC-HCl, with only the Lys residue being crosslinked. (B) HPLC traces recording UV 260 nm absorbance of reaction products during a 10 h time course of a model condensation reaction at pH 8. Peaks corresponding to AMP (highlighted blue), Pep1, and crosslinking product Amp-Pep1 (highlighted red), 1-methylimidazole (1-Melm) are marked. Reaction times and product yields are indicated. (C) The highest product yield was achieved at pH 8.

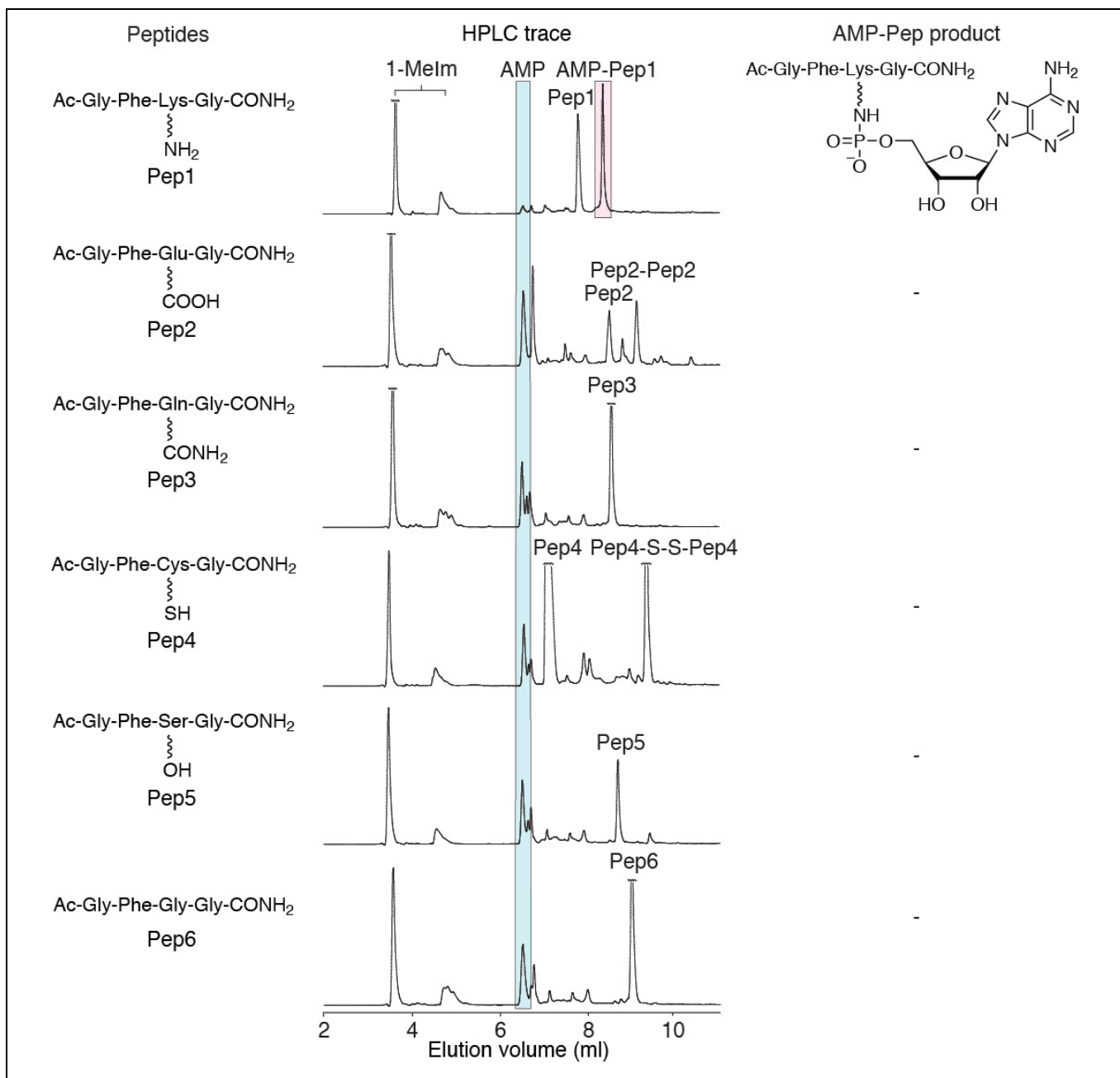


Fig. S6. Specificity of EDC-mediated condensation reaction. When six different peptides of similar sequence, Acetyl-N-Gly-Phe-X-Gly-CO-NH₂ (X = Lys, Glu, Gln, Cys, Ser, or Gly), were incubated with AMP and EDC-HCl for 10 h at 50 °C, only peptide Pep1 with Lys residue was detected to form phosphoamide product indicating that EDC crosslinking is primarily amino-group-specific. Peaks corresponding to AMP (highlighted blue), Pep1, Pep2, Pep3, Pep4, Pep5, Pep6, crosslinking product Amp-Pep1 (highlighted red) product, 1-methylimidazole (1-Melm) and non-phosphoamide product Pep2-Pep2 (an anhydride dimer, see also Fig. S9) and Pep4-S-S-Pep4 (a dimer formed by disulfide bridge) are marked.

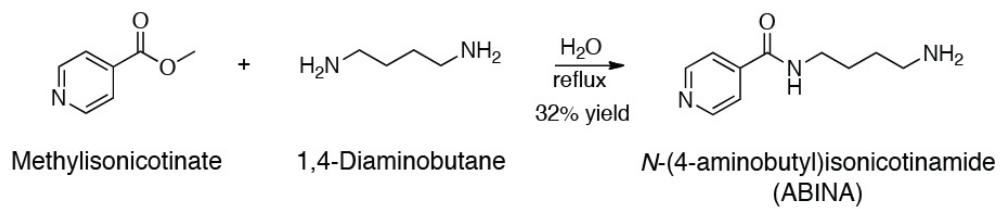


Fig. S7. Schematic diagram of ABINA synthesis. ABINA is a highly soluble UV-absorbing compound that was prepared by refluxing methylisonicotinate and 1,4-diaminobutane in water (see Materials and Methods).

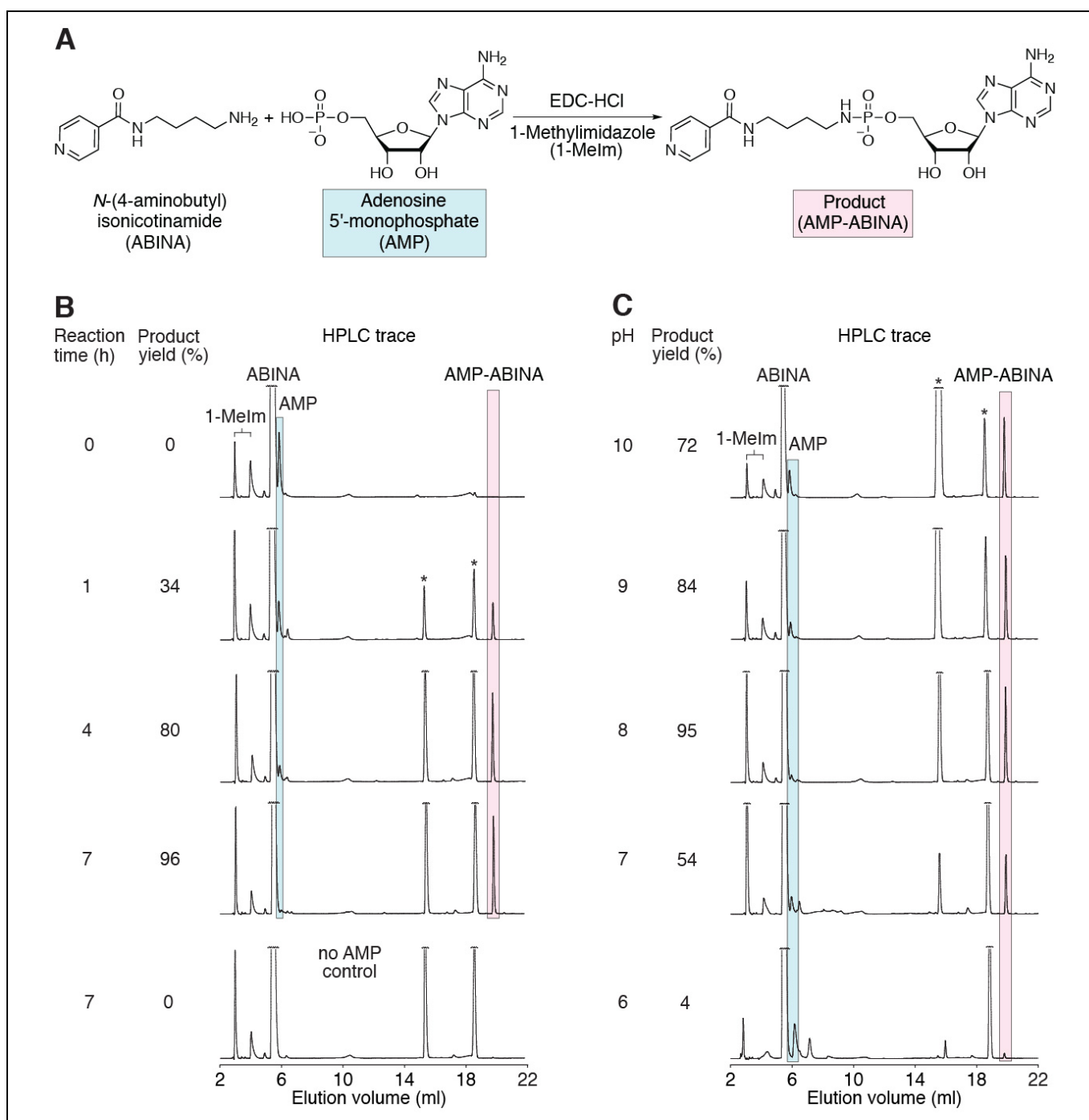


Fig. S8. Carbodiimide-mediated condensation using UV-absorbing model compounds. (A) The reaction between AMP and ABINA at 50 °C yielded a stable phosphoamide product AMP-ABINA. **(B)** HPLC traces recording UV 260 nm absorbance of reaction products during a 7 h time course of a model condensation reaction at pH 8. Peaks corresponding to AMP (highlighted blue), ABINA, crosslinking product AMP-ABINA (highlighted red), 1-methylimidazole (1-Melm) and side products (*) are marked. Reaction times and product yields are indicated. The crosslink (XL) product reverted to AMP and ABINA upon incubation in 80% acetic acid, as expected for a phosphoamide (data not shown). **(C)** The highest yield (95%) of AMP-ABINA occurred at pH 8.

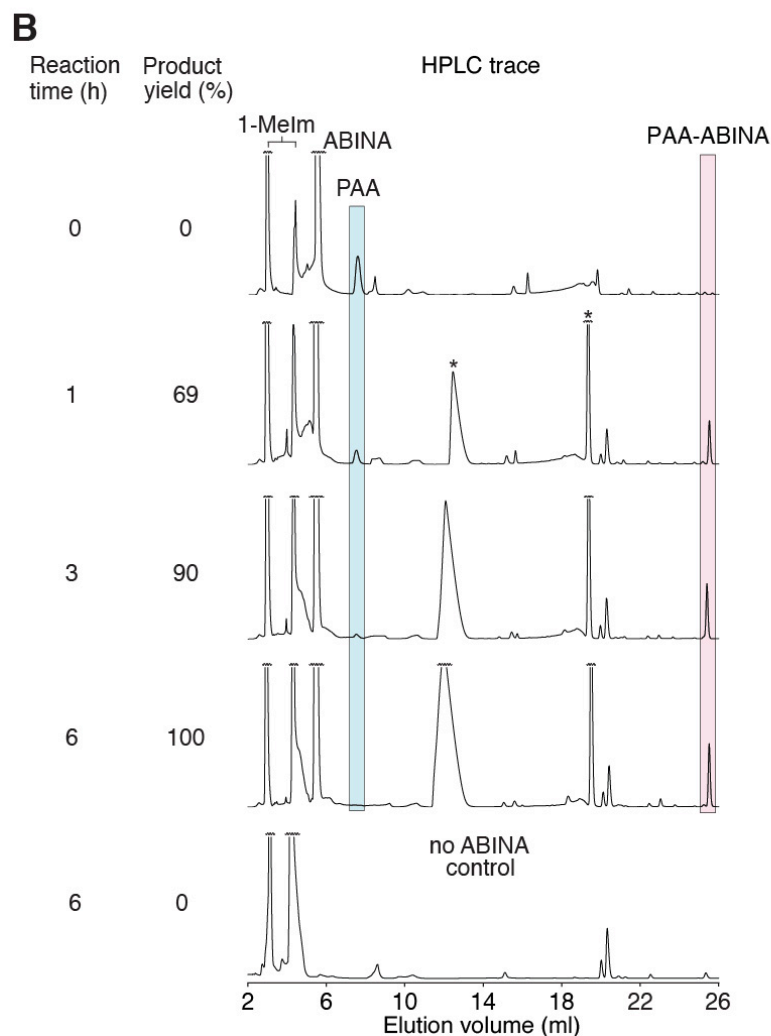
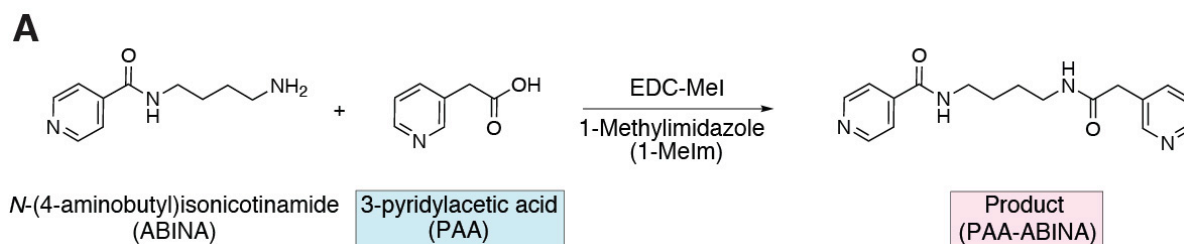


Fig. S9. EDC-based condensation of ABINA and PAA indicating EDC-based crosslinking between proteins. (A) The reaction between PAA and ABINA at 50 °C yielded a stable carboxylic acid amide product PAA-ABINA. (B) HPLC traces recording UV 260 nm absorbance of reaction products during a 6 h time course of a model condensation reaction at pH 8. EDC-Mel was used in place of EDC-HCl, resulting in a substantial decrease in reaction time. The 6 h completion time for amide bond formation is twice that for phosphoamide bond formation under the same reaction conditions, indicating that phosphoamide bond formation is favored over amide bond formation. Peaks corresponding to synthesized amine ABINA, PAA (highlighted blue) and crosslinking product PAA-ABINA (highlighted red), 1-methylimidazole (1-Melm) and side products (*) are marked. Reaction times and product yields are indicated. When the condensation reaction proceeded without ABINA (no ABINA control), anhydride product formation was observed.

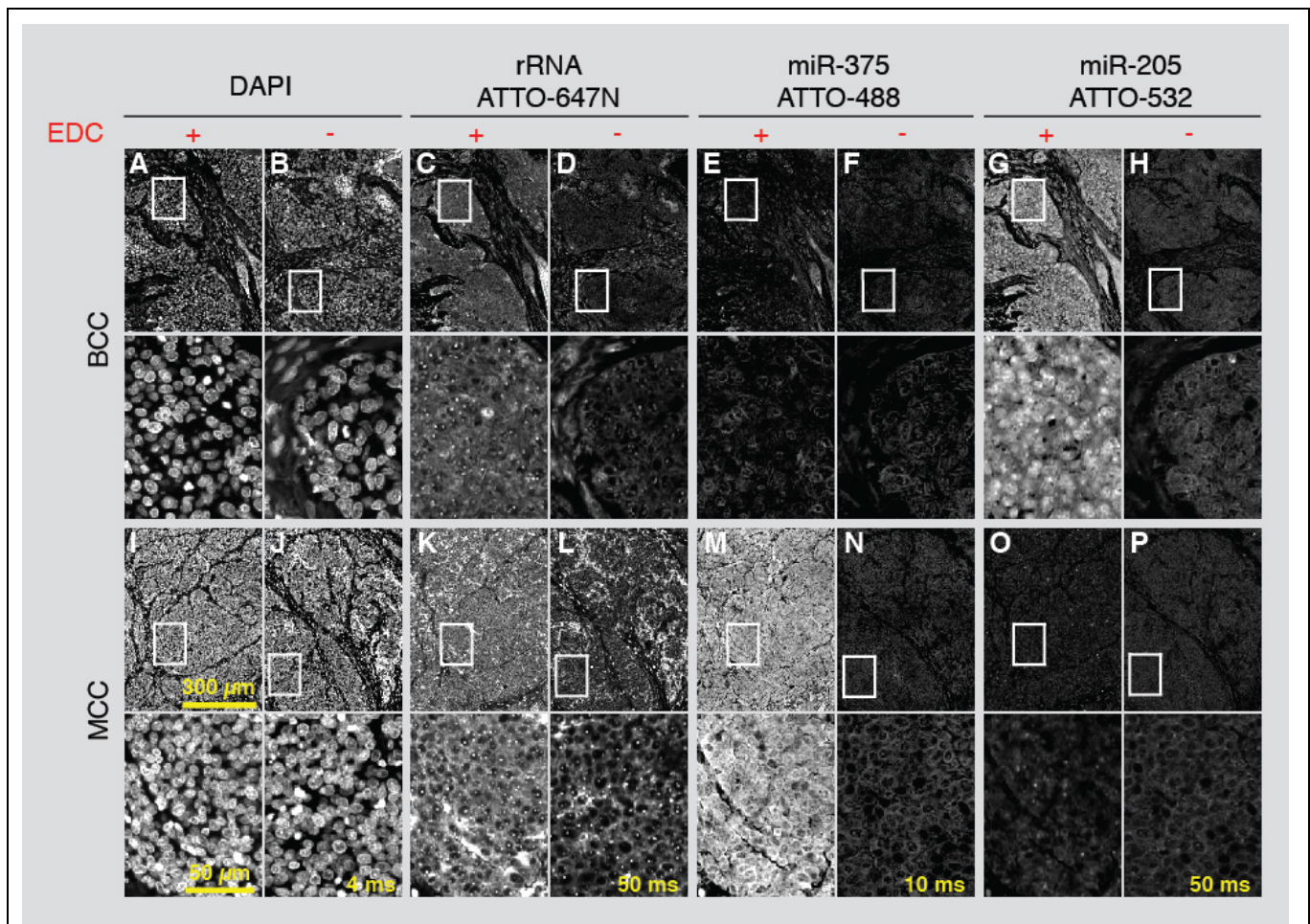
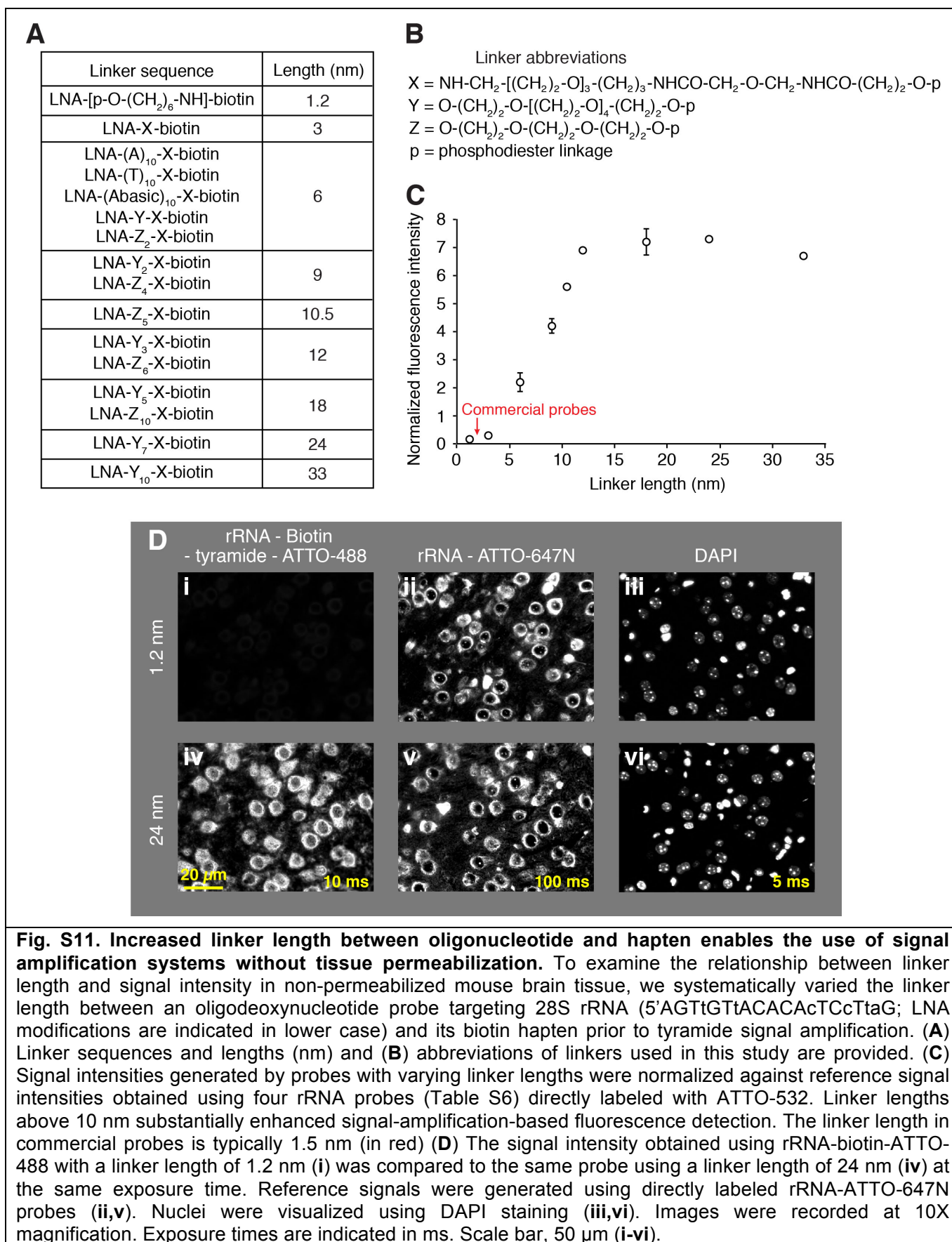


Fig. S10. EDC-based retention of long (rRNA) and short (miRNA) RNAs in FFPE tissues. Multicolor miRNA FISH was performed on BCC and MCC tissues with (+) and without (-) EDC fixation. rRNA signals were brighter in EDC-fixed (C,K) than unfixed (D,L) tissues, indicating retention. miR-205 and miR-375 signals were identified as expected in EDC-fixed (E,G,M,O) but not unfixed (F,H,N,P) tissues. Images were recorded at 60X magnification. Exposure times are indicated in ms. Scale bar, 300 μ m, for insert 50 μ m (A-P).



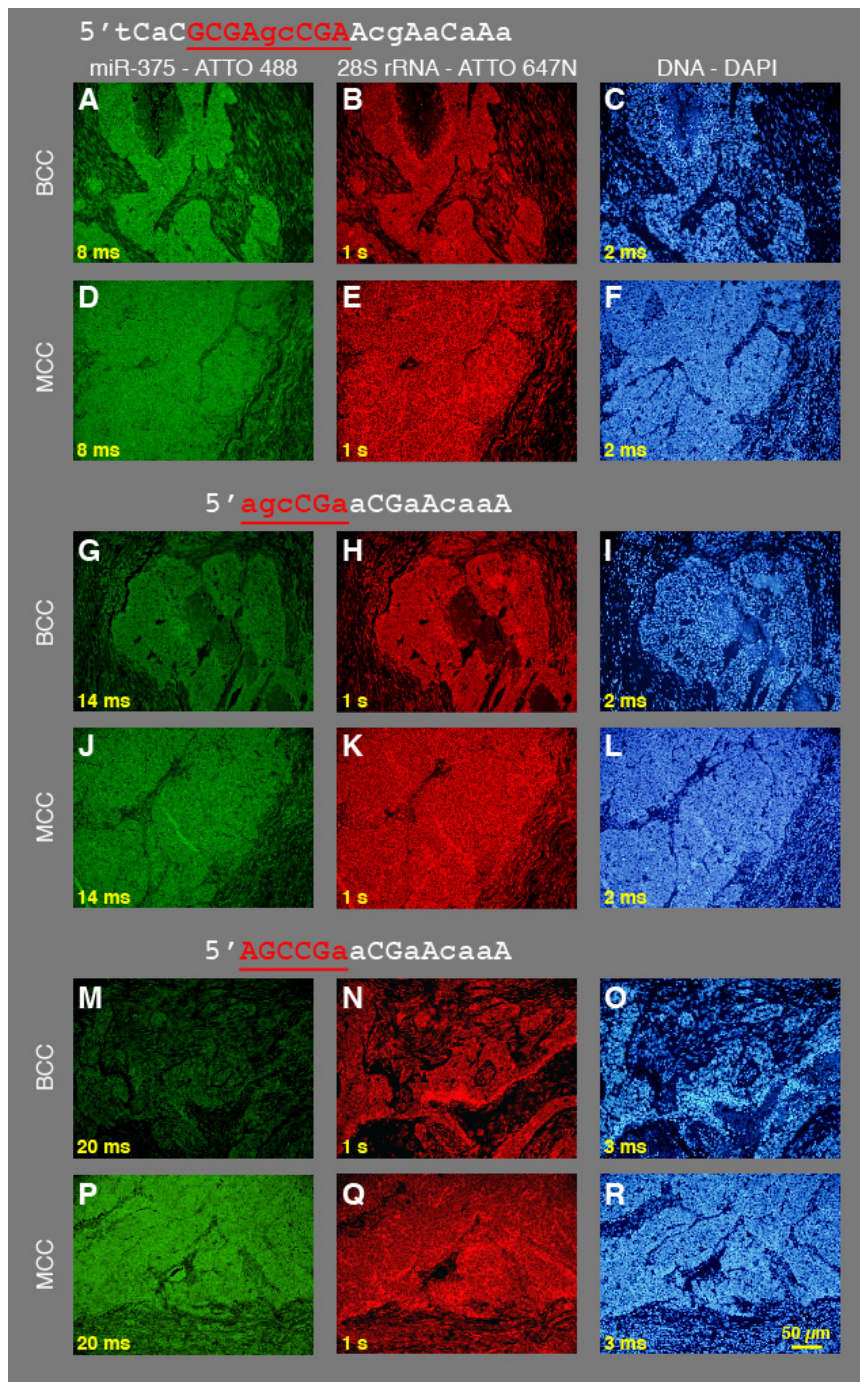


Fig. S12. miR-375 LNA-probe design. miR-375 (**A,D,G,J,M,P**) and 28S rRNA (**B,E,H,K,N,Q**) hybridization patterns in BCC and MCC tissues were used to assess probe specificity. Probe sequence matches to 28S rRNA are highlighted and underlined in red; LNA modifications are indicated in lower case. Antisense miR-375 LNA probe (22 nt, plus 25 nm linker) was detected in (**A**) BCC and (**D**) MCC, indicating rRNA mishybridization. Antisense miR-375 LNA probe (15 nt, plus 25 nm linker), with a short (6 nt) sequence match with rRNA, was detected in (**G**) BCC and (**J**) MCC, again indicating mishybridization. Removal of three LNA modifications from the region of sequence similarity (third probe sequence) resulted in a substantial decrease (11 °C) in melting temperature, and a specific miR-375 signal (**M**) BCC and (**P**) MCC). Nuclei were visualized using DAPI staining (**C,F,I,L,O,R**). Images were recorded at 20X magnification. Exposure times are indicated in ms or s. Scale bar, 50 μm (**A-R**).

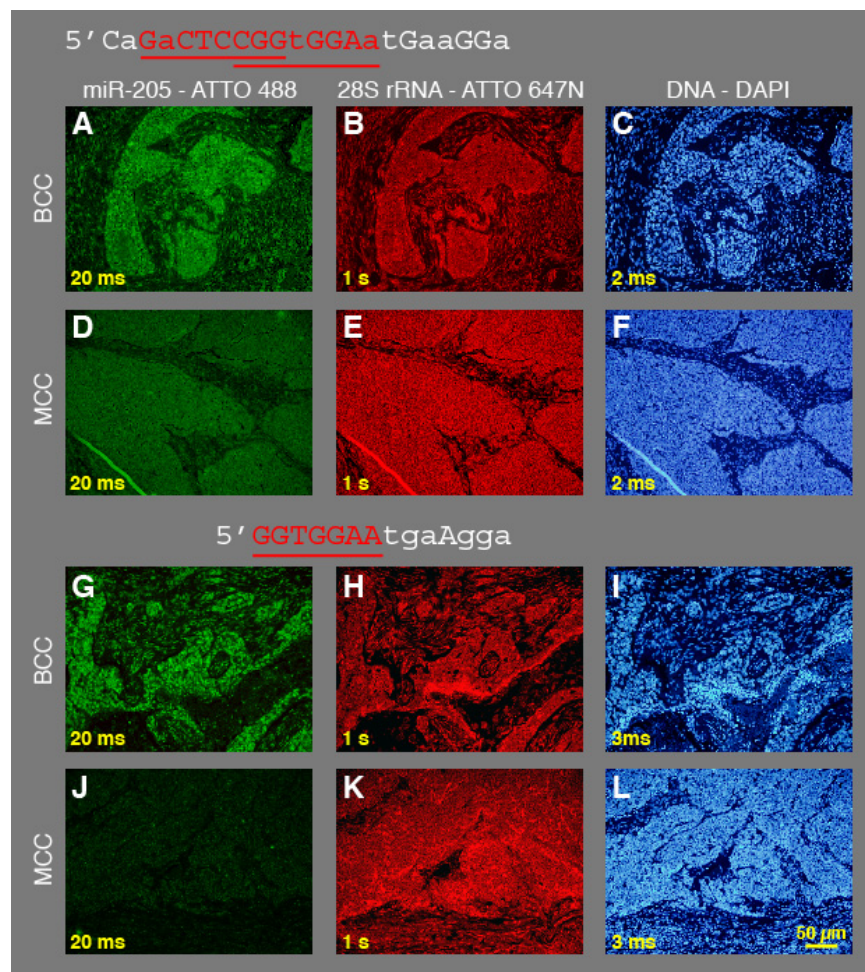


Fig. S13. miR-205 LNA-probe design. miR-205 (**A,D,G,J**) and 28S rRNA (**B,E,H,K**) hybridization patterns in BCC and MCC tissues were used to assess probe specificity. Probe sequence matches to 28S rRNA are highlighted and underlined in red; LNA modifications are indicated in lower case. Antisense miR-205 LNA probe (22 nt, plus 25 nm linker) was detected in (**A**) BCC and (**D**) MCC indicating rRNA mishybridization. Shortening the probe sequence and removal of LNA modifications from the region of sequence similarity, resulted in a substantial decrease (9 °C) in melting temperature, and specific miR-205 signal in BCC (**G,J**). Nuclei were visualized using DAPI staining (**C,F,I,L**). Images were recorded at 20X magnification. Exposure times are indicated in ms or s. Scale bar, 50 μm (**A-L**).

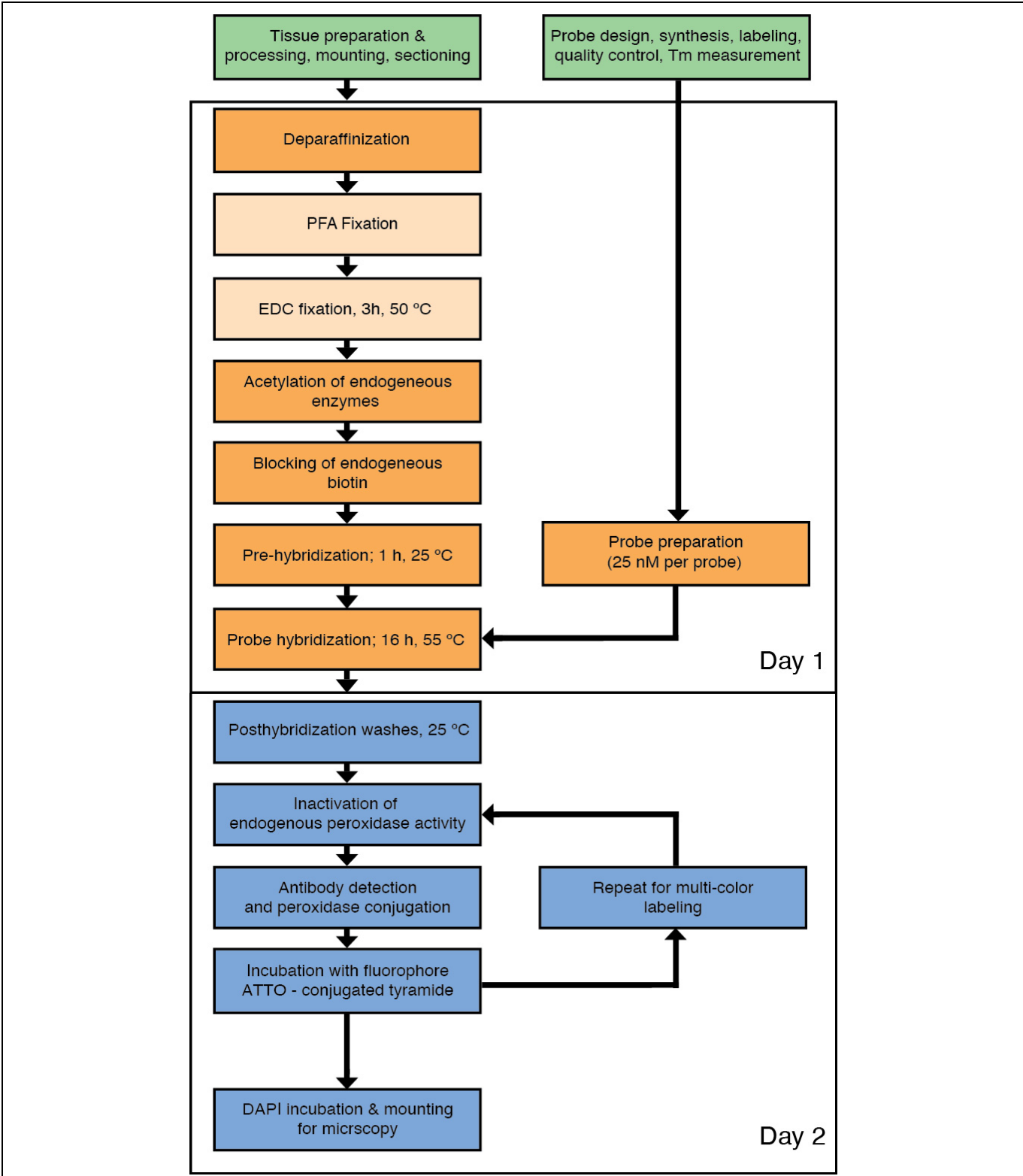


Fig. S14. Workflow diagram of optimized miRNA FISH protocol.

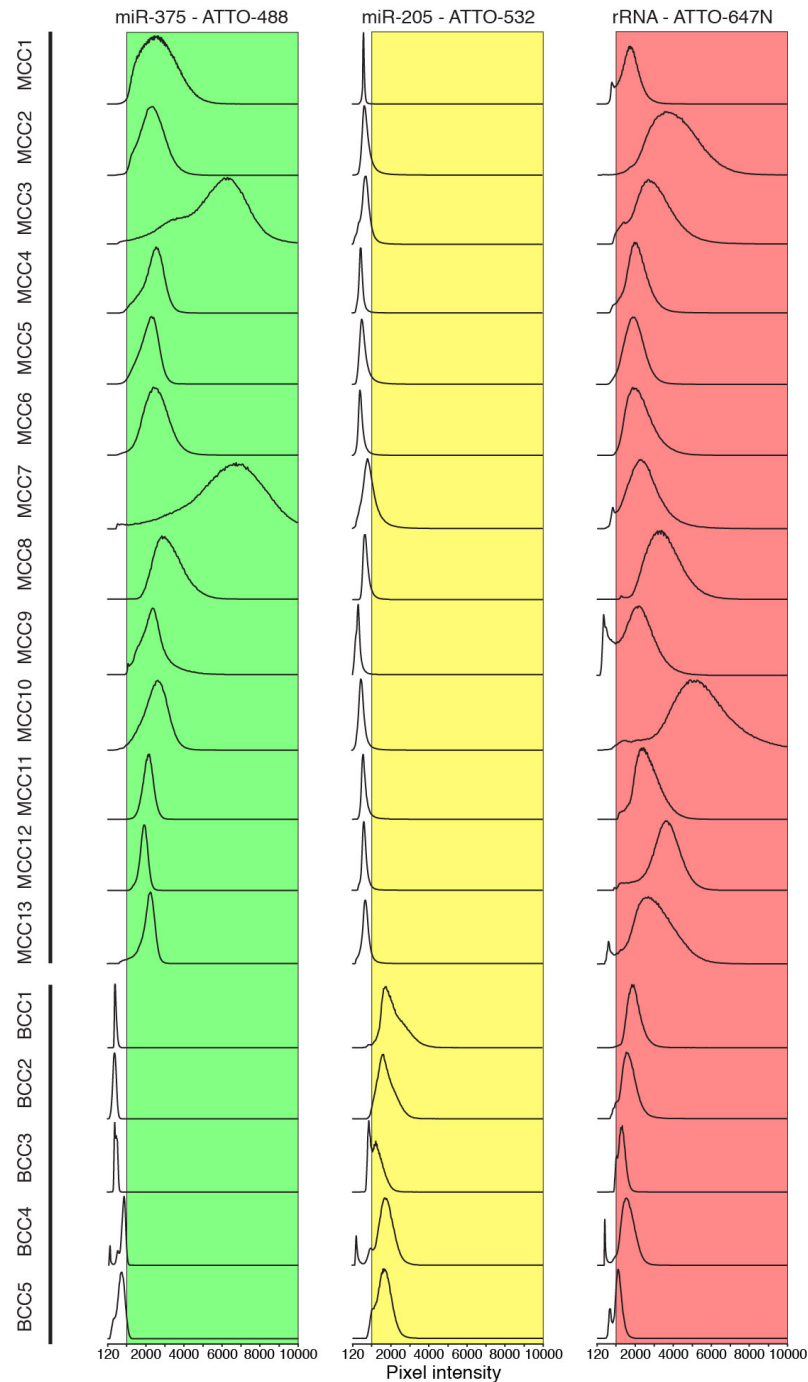


Fig. S15. miRNA signal normalization and establishment of cut-off values for tumor differentiation.

Signal intensity histograms for miR-375-ATTO-488, miR-205-ATTO-532, and rRNA-ATTO-647N were used to delineate and differentiate specific RNA and background signals; cut-off values were established on a pilot set of tumors (BCC1 and MCC1) and set to a pixel intensity of 1,000 for miR-375, miR-205, and rRNA. Corrected miR-375, miR-205, and rRNA fluorescence signals (respectively indicated by green, yellow, and red boxes) were multiplied by their corresponding integral of pixel intensities and these values were used to normalize miRNA against reference rRNA signals. Blinded analysis of 16 BCC and MCC tumors was performed using the same cut-off values as above and all tumors were correctly identified based on normalized miR-205 and miR-375 signals; signal intensity histograms from pilot (BCC1 and MCC1) and (BCC2-13 and MCC2-5) tumors are presented. The Y-axis is not shown here, instead sum of pixels above a defined threshold as seen in Table S7.

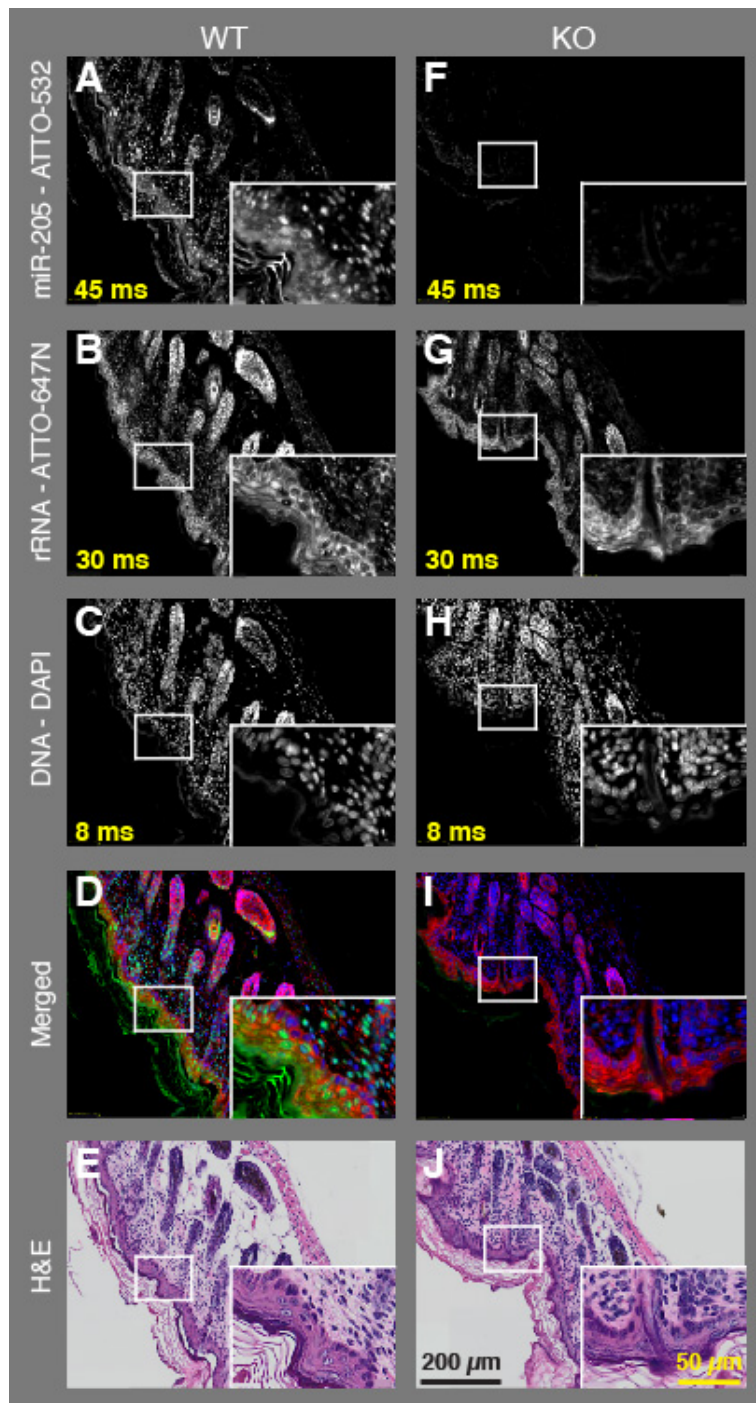


Fig. S16. Confirmation of miR-205 probe specificity in mouse skin tissues. Parallel detection of miR-205 and 28S rRNA in FFPE skin tissue sections from wild-type (WT) and miR-205 knockout (KO) mice using multicolor miRNA FISH. Probes and reaction conditions were identical to those used in Fig. 2. miR-205 signal was present in WT (A) but not KO (F) skin tissues. 28S rRNA signals were similar for WT and KO tissues (B,G). Nuclei were visualized using DAPI staining (C,H). Merged images (D,I) show miR-205 signals in epidermis, hair follicles, and a dermal cell subpopulation (in green), rRNA signals (in red), and nuclei (in blue). H&E stained WT and KO skin tissues (E,J) are histologically indistinguishable. Images were recorded at 20X magnification. Representative areas, indicated by white rectangles, are shown at 60X magnification to illustrate signal localization. Exposure times are indicated in ms. Scale bar, 200 μm , for insert, 50 μm (A-J).

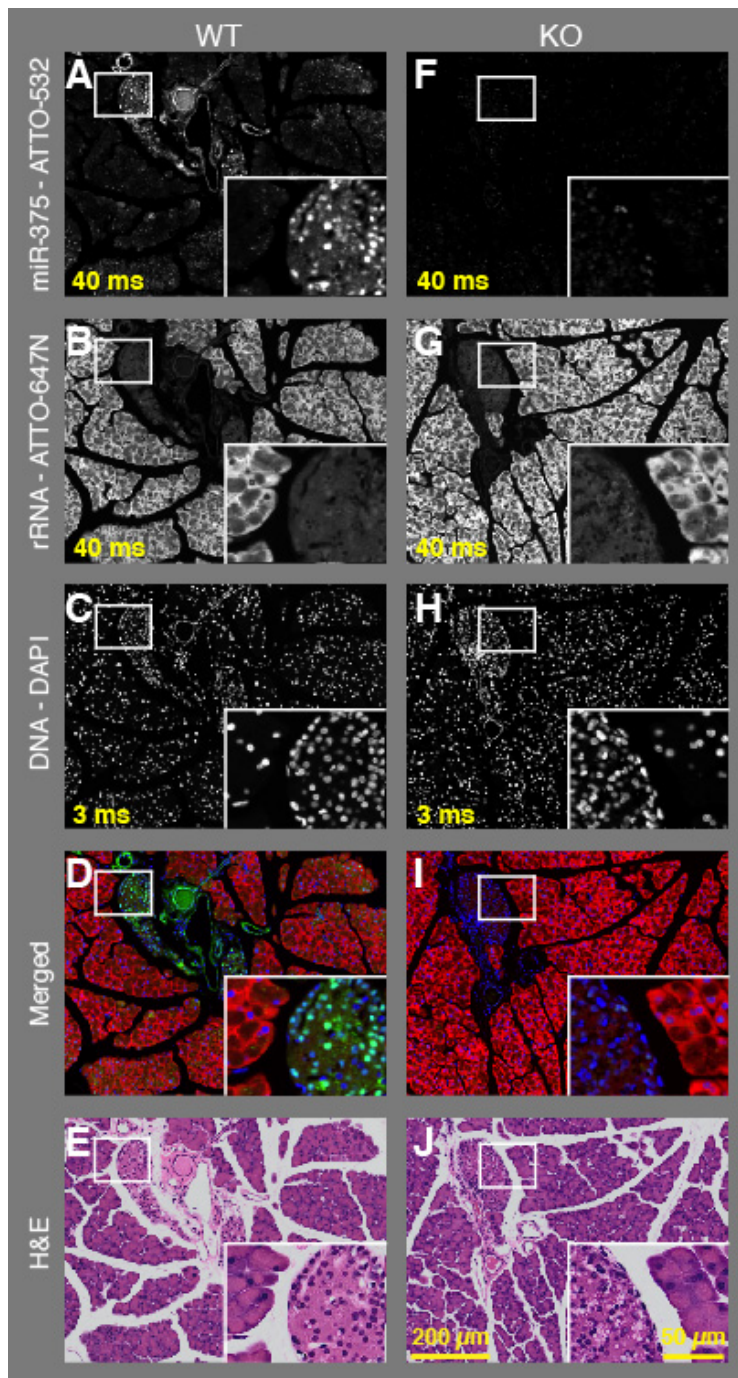


Fig. S17. Confirmation of miR-375 probe specificity in mouse pancreas tissues. Parallel detection of miR-375 and 28S rRNA in FFPE pancreatic tissue sections from wild-type (WT) and miR-375 knockout (KO) mice using multicolor miRNA FISH. Probes and reaction conditions were identical to those used in Fig. 2. miR-375 signal was present in WT (A) but not KO (F) pancreatic islets and ductal epithelium. 28S rRNA signals were similar for WT and KO tissues (B,G). Nuclei were visualized using DAPI staining (C,H). Merged images (D,I) show miR-375 signals in pancreatic islets and ductal epithelium (in green), rRNA signals (in red), and nuclei (in blue). H&E stained WT and KO pancreas tissues (E,J) are histologically indistinguishable. Images were recorded at 20X magnification. Representative areas, indicated by white rectangles, are shown at 60X magnification to illustrate signal localization. Exposure times are indicated in ms. Scale bar, 200 μm , for insert, 50 μm (A-J).

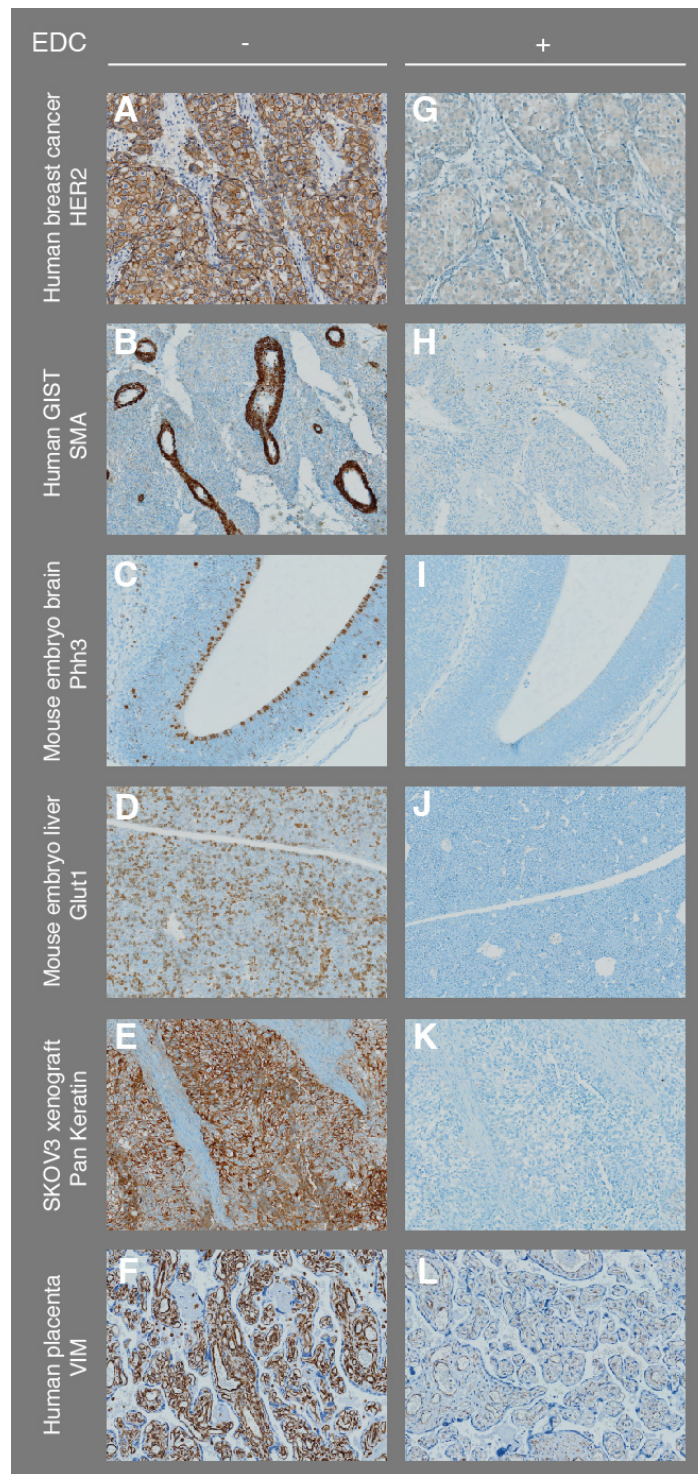


Fig. S18. EDC fixation is incompatible with immunohistochemical staining. To assess the compatibility of EDC-based RNA fixation with immunohistochemistry, we tested multiple EDC-fixed and unfixed tissue sections with commercial grade antibodies. Appropriate signals for human epidermal growth factor receptor 2 (HER2), smooth muscle actin (SMA), phospho-histone-H3 (Phh3), glucose transporter 1 (Glut1), pan-keratin, and vimentin (VIM) were respectively seen in human breast cancer, human gastrointestinal stromal tumor (GIST), mouse embryonic brain, mouse embryonic liver, SKOV3 xenograft, and human placental tissues in unfixed (**A-F**) but not EDC-fixed (**G-L**) tissue sections.

Sample name	Sample type	Year of fixation	RNA extraction method	Spectrophotometer	Total RNA concentration (µg/µl)	A260/A280 ratio	RNA integrity	Immunostaining	MCV status	% tumor
MCC1	FFPE tissue punch	2008	Ambion Recoverall	Nanodrop	1.00	1.92	Partially degraded	CK20+, CHR+, SYN+	Negative	75
MCC2	FFPE tissue punch	2008	Ambion Recoverall	Nanodrop	0.88	2.00	Partially degraded	CK20+	Positive	25
MCC3	FFPE tissue punch	2007	Ambion Recoverall	Nanodrop	1.12	2.00	Partially degraded	CK20+, S100-	Negative	75
MCC4	FFPE tissue punch	2005	Ambion Recoverall	Nanodrop	1.24	1.94	Partially degraded	CK20+, CK7+, S100+	Positive	50
MCC5	FFPE tissue punch	2006	Ambion Recoverall	Nanodrop	0.96	2.00	Partially degraded	CK20+, EMA+	Negative	75
MCC6	FFPE tissue punch	2005	Ambion Recoverall	Nanodrop	0.64	2.00	Partially degraded	CK20+, LCA-	Positive	90
MCC7	FFPE tissue punch	2006	Ambion Recoverall	Nanodrop	0.88	2.00	Partially degraded	CK20+, CK7-, SYN+	Positive	75
MCC8	FFPE tissue punch	2005	Ambion Recoverall	Nanodrop	0.44	1.83	Partially degraded	CK20-, LMWK+, SYN+	Negative	60
MCC9	FFPE tissue punch	2005	Ambion Recoverall	Nanodrop	2.44	1.91	Partially degraded	CK20+, CK7-, CHR+, LMWK+, SYN+, TTF1-	Positive	75
MCC10	FFPE tissue punch	2004	Ambion Recoverall	Nanodrop	1.28	1.88	Partially degraded	CK20-, CK7+, CHR+, LMWK+, NSE+, S100-	Positive	95
MCC11	FFPE tissue punch	2003	Ambion Recoverall	Nanodrop	0.56	2.00	Partially degraded	CK20+, LMWK+	Indeterminate	95
MCC12	FFPE tissue punch	2001	Ambion Recoverall	Nanodrop	1.20	2.00	Partially degraded	CK20+, CK7-, CEA+, Chr+, LMWK+, NSE+, SYN+	Positive	90
NS1	FFPE tissue punch	2008	Ambion Recoverall	Nanodrop	0.28	1.75	Partially degraded	NT	Positive	NA
NS2	FFPE tissue punch	2007	Ambion Recoverall	Nanodrop	0.36	1.80	Partially degraded	NT	Indeterminate	NA
NS3	FFPE tissue punch	2005	Ambion Recoverall	Nanodrop	0.36	2.25	Partially degraded	NT	Indeterminate	NA
NS4	FFPE tissue punch	2006	Ambion Recoverall	Nanodrop	0.36	2.25	Partially degraded	NT	Negative	NA
BCC1	FFPE tissue punch	2008	Ambion Recoverall	Nanodrop	0.28	1.75	Partially degraded	NT	Negative	20
BCC2	FFPE tissue punch	2008	Ambion Recoverall	Nanodrop	0.52	2.17	Partially degraded	NT	Negative	75
BCC3	FFPE tissue punch	2008	Ambion Recoverall	Nanodrop	1.12	2.00	Partially degraded	NT	Negative	95
BCC4	FFPE tissue punch	2008	Ambion Recoverall	Nanodrop	0.28	2.33	Partially degraded	NT	Negative	75
MCC13a	FFPE tissue roll ⁵⁰	2007	Epicenter Masterpure	SmartSpec	0.48	1.50	Partially degraded	CK20+, CHR+, SYN+, NF-, TTF1-	NT	80
MCC13b	FFPE tissue roll ¹⁵⁰	2007	Epicenter Masterpure	SmartSpec	0.64	1.60	Partially degraded	CK20+, CHR+, SYN+, NF-, TTF1-	NT	80
MCC14a	FFPE tissue roll ⁵⁰	2007	Epicenter Masterpure	SmartSpec	1.40	1.75	Partially degraded	CK20+, CK7-, NSE+	NT	80
MCC14b	FFPE tissue roll ¹⁵⁰	2007	Epicenter Masterpure	SmartSpec	1.80	1.73	Partially degraded	CK20+, CK7-, NSE+	NT	80
NS5a	FFPE tissue roll ⁵⁰	2008	Epicenter Masterpure	SmartSpec	0.01	1.00	Partially degraded	NT	NT	NA
NS5b	FFPE tissue roll ¹⁵⁰	2008	Epicenter Masterpure	SmartSpec	0.08	2.00	Partially degraded	NT	NT	NA
BCC5a	FFPE tissue roll ⁵⁰	2008	Epicenter Masterpure	SmartSpec	0.44	1.83	Partially degraded	NT	NT	80
BCC5b	FFPE tissue roll ¹⁵⁰	2008	Epicenter Masterpure	SmartSpec	0.52	1.63	Partially degraded	NT	NT	80
MKL-1a	Cell line	Not fixed	TRIzol Reagent	SmartSpec	0.83	1.59	Intact	NT	Positive	NA
MCC13	Cell line	Not fixed	TRIzol Reagent	SmartSpec	0.93	1.64	Intact	NT	Negative	NA
MCC26	Cell line	Not fixed	TRIzol Reagent	SmartSpec	0.81	1.98	Intact	NT	Negative	NA
MS-1	Cell line	Not fixed	TRIzol Reagent	SmartSpec	0.94	1.73	Intact	NT	Positive	NA
MKL-1b	Cell line	Not fixed	TRIzol Reagent	SmartSpec	1.47	1.61	Intact	NT	Positive	NA
UIS0	Cell line	Not fixed	TRIzol Reagent	SmartSpec	2.90	1.68	Intact	NT	Negative	NA
MKL-1c	Cell line	Not fixed	TRIzol Reagent	SmartSpec	2.03	1.60	Intact	NT	Positive	NA
MKL-2	Cell line	Not fixed	TRIzol Reagent	SmartSpec	3.65	NA	Intact	NT	Positive	NA

Table S1. Total RNA isolation from clinical samples. Total RNA was isolated from FFPE BCC, MCC (ten primary and two metastatic), and NS tissues, and freshly cultured MCC-derived cell lines using three different RNA extraction methods. Sample replicates are denoted by the suffixes a-c. FFPE tissue roll thickness in µm is indicated in superscript. Immunohistochemical staining was performed for carcinoembryonic antigen (CEA), chromogranin (CHR), cytokeratin 7 (CK7), cytokeratin 20 (CK20), epithelial membrane antigen (EMA), leukocyte common antigen (LCA), low molecular weight keratin (LMWK), neuron-specific enolase (NSE), neurofilament (NF), synaptophysin (SYN), and thyroid transcription factor 1 (TTF-1). MCV status is indicated where available. NA denotes measurement not available. NT denotes sample not tested.

Sample name	Sequencing run	Total reads	Calibrator	miRNA	% miRNA	None	% None	rRNA	% rRNA	tRNA	% tRNA	MiscRNA	% MiscRNA	Marker	% Marker
MCC1	1	346,160	213,307	108,829	81.9	10,084	7.6	6,248	4.7	5,886	4.4	1,776	1.3	30	0.0
MCC2	1	269,529	163,966	83,392	79.0	7,473	7.1	6,374	6.0	6,150	5.8	2,140	2.0	34	0.0
MCC3	1	463,784	184,674	237,241	85.0	19,242	6.9	8,428	3.0	10,696	3.8	3,494	1.3	9	0.0
MCC4	1	508,423	223,255	233,477	81.9	16,275	5.7	16,475	5.8	15,188	5.3	3,748	1.3	5	0.0
MCC5	1	397,029	209,520	143,956	76.8	13,934	7.4	17,040	9.1	8,264	4.4	4,309	2.3	6	0.0
MCC6	1	433,934	220,098	150,143	70.2	18,766	8.8	23,286	10.9	14,475	6.8	7,140	3.3	26	0.0
MCC7	1	306,621	158,251	118,650	80.0	10,787	7.3	8,866	6.0	7,954	5.4	2,109	1.4	4	0.0
MCC8	1	401,743	191,748	163,928	78.1	13,317	6.3	15,339	7.3	14,603	7.0	2,802	1.3	6	0.0
MCC9	1	418,710	211,000	144,291	69.5	20,148	9.7	19,985	9.6	15,838	7.6	7,433	3.6	15	0.0
MCC10	1	475,659	231,104	138,293	56.5	36,767	15.0	35,390	14.5	22,043	9.0	12,053	4.9	9	0.0
MCC11	1	351,074	177,461	119,249	68.7	17,200	9.9	19,685	11.3	13,397	7.7	4,056	2.3	26	0.0
MCC12	1	275,277	145,448	71,379	55.0	11,952	9.2	28,093	21.6	13,629	10.5	4,769	3.7	7	0.0
NS1	1	326,487	183,158	122,368	85.4	6,377	4.4	8,055	5.6	5,574	3.9	916	0.6	39	0.0
NS2	1	121,271	65,628	47,771	85.9	2,637	4.7	2,968	5.3	1,869	3.4	375	0.7	23	0.0
NS3	1	227,023	129,939	67,506	69.5	6,238	6.4	12,847	13.2	9,189	9.5	1,275	1.3	29	0.0
NS4	1	371,336	207,777	130,295	79.7	7,930	4.8	16,369	10.0	7,316	4.5	1,620	1.0	29	0.0
BCC1	1	413,375	183,123	206,096	89.5	10,338	4.5	6,741	2.9	5,321	2.3	1,708	0.7	48	0.0
BCC2	1	447,357	207,843	217,614	90.9	10,233	4.3	4,929	2.1	5,456	2.3	1,251	0.5	31	0.0
BCC3	1	478,255	217,634	239,447	91.9	11,100	4.3	5,586	2.1	2,774	1.1	1,680	0.6	34	0.0
BCC4	1	556,983	218,261	308,249	91.0	10,758	3.2	10,479	3.1	7,256	2.1	1,942	0.6	38	0.0
MCC13a	2	487,374	175,626	207,241	66.5	22,355	7.2	32,641	10.5	39,965	12.8	8,562	2.7	984	0.3
MCC13b	2	398,202	124,388	185,175	67.6	19,730	7.2	27,854	10.2	32,462	11.9	7,745	2.8	848	0.3
MCC14a	2	309,206	144,867	101,900	62.0	26,961	16.4	12,085	7.4	18,601	11.3	4,422	2.7	370	0.2
MCC14b	2	193,092	152,228	18,724	45.8	10,299	25.2	5,050	12.4	4,597	11.2	2,123	5.2	71	0.2
NS5a	2	242,202	204,422	27,485	72.8	3,575	9.5	2,911	7.7	3,097	8.2	385	1.0	327	0.9
NS5b	2	245,432	201,504	31,921	72.7	3,577	8.1	2,902	6.6	3,929	8.9	329	0.7	1180	2.7
BCC5a	2	649,145	162,406	401,500	82.5	14,056	2.9	29,980	6.2	35,735	7.3	4,876	1.0	592	0.1
BCC5b	2	550,843	168,053	319,302	83.4	13,450	3.5	17,556	4.6	28,533	7.5	3,666	1.0	283	0.1
MKL-1a	2	537,400	139,582	361,783	90.9	15,625	3.9	3,426	0.9	12,297	3.1	3,906	1.0	781	0.2
MCC13	2	372,321	140,958	216,455	93.6	7,382	3.2	679	0.3	5,480	2.4	719	0.3	648	0.3
MCC26	2	327,222	177,471	130,675	87.3	9,115	6.1	1,270	0.8	6,055	4.0	1,167	0.8	1469	1.0
MS-1	2	588,386	107,475	448,106	93.2	13,167	2.7	4,138	0.9	8,737	1.8	5,698	1.2	1065	0.2
MKL-1b	2	645,227	152,483	434,595	88.2	21,066	4.3	4,679	0.9	17,223	3.5	13,920	2.8	1261	0.3
UIS0	2	364,004	199,572	150,539	91.6	7,813	4.8	1,108	0.7	2,873	1.7	676	0.4	1423	0.9
MKL-1c	2	358,960	138,724	197,841	89.8	10,119	4.6	2,827	1.3	5,404	2.5	2,903	1.3	1142	0.5
MKL-2	2	391,740	168,396	190,566	85.3	12,265	5.5	3,277	1.5	12,951	5.8	3,082	1.4	1203	0.5

Table S2. Small RNA sequence read counts and annotation. miRNA expression profiles were generated for all 36 samples in two barcoded sequencing runs. Total sequence reads per sample averaged 395,855 (range: 121,271-649,145) and were similar for each run, respectively averaging 379,502 (range: 121,271-556,983) and 416,297 (range: 193,092-649,145) sequence reads. Following barcode extraction, sequence reads were annotated into the following RNA categories: calibrator (spiked in calibrator oligoribonucleotides for miRNA quantitation), miRNA, none (sequences with unclear or no match to the human genome), rRNA, tRNA, miscellaneous RNA (miscRNA: poorly annotated non-coding RNA transcripts), and marker RNA (size marker RNAs that were used for isolating ligation products during cDNA library preparation). Following annotation, miRNA was the most abundant (average 78.9%, range: 45.8-93.6%) RNA class in each sample. The sum of proportions may not equal 100 due to rounding errors.

Sample name	Calibrator reads	miRNA reads	miRNA:calibrator read ratio	Calibrator:total RNA conc. ratio (fmol/ μ g)	Total miRNA conc. (fmol/ μ g)	miR-375 reads	% miR-375/total miRNA reads	miR-375 conc. (amol/ μ g)	miR-205 reads	% miR-205/total miRNA reads	miR-205 conc. (amol/ μ g)	relative miR-375 expression level
MCC1	213,307	108,829	0.51	10	5.1	6,758	6.2	316.8	318	0.3	14.9	NT
MCC2	163,966	83,392	0.51	10	5.1	8,773	10.5	535.0	16	0.0	1.0	462.0
MCC3	184,674	237,241	1.28	10	12.8	29,789	12.6	1613.1	24	0.0	1.3	878.0
MCC4	223,255	233,477	1.05	10	10.5	15,951	6.8	714.5	159	0.1	7.1	377.0
MCC5	209,520	143,956	0.69	10	6.9	1,929	1.3	92.1	11	0.0	0.5	43.2
MCC6	220,098	150,143	0.68	10	6.8	11,686	7.8	530.9	17	0.0	0.8	448.0
MCC7	158,251	118,650	0.75	10	7.5	10,842	9.1	685.1	10	0.0	0.6	300.0
MCC8	191,748	163,928	0.85	10	8.5	3,051	1.9	159.1	3,425	2.1	178.6	103.0
MCC9	211,000	144,291	0.68	10	6.8	15,488	10.7	734.0	31	0.0	1.5	399.0
MCC10	231,104	138,293	0.60	10	6.0	6,229	4.5	269.5	14	0.0	0.6	293.0
MCC11	177,461	119,249	0.67	10	6.7	4,537	3.8	255.6	18	0.0	1.0	141.0
MCC12	145,448	71,379	0.49	10	4.9	2,938	4.1	202.0	5	0.0	0.3	228.0
NS1	183,158	122,368	0.67	10	6.7	61	0.0	3.3	10,064	8.2	549.5	2.0
NS2	65,628	47,771	0.73	10	7.3	10	0.0	1.5	3,541	7.4	539.6	1.2
NS3	129,939	67,506	0.52	10	5.2	8	0.0	0.6	3,750	5.6	288.6	0.6
NS4	207,777	130,295	0.63	10	6.3	46	0.0	2.2	10,198	7.8	490.8	1.0
BCC1	183,123	206,096	1.13	10	11.3	8	0.0	0.4	16,474	8.0	899.6	NT
BCC2	207,843	217,614	1.05	10	10.5	7	0.0	0.3	8,881	4.1	427.3	NT
BCC3	217,634	239,447	1.10	10	11.0	3	0.0	0.1	18,213	7.6	836.9	NT
BCC4	218,261	308,249	1.41	10	14.1	11	0.0	0.5	17,992	5.8	824.3	NT
MCC13a	175,626	207,241	1.18	10	11.8	16,073	7.8	915.2	18	0.0	1.0	NT
MCC13b	124,388	185,175	1.49	10	14.9	16,179	8.7	1300.7	25	0.0	2.0	NT
MCC14a	144,867	101,900	0.70	10	7.0	13,897	13.6	959.3	148	0.1	10.2	NT
MCC14b	152,228	18,724	0.12	10	1.2	13,888	74.2	912.3	1	0.0	0.1	NT
NS5a	204,422	27,485	0.13	100	13.4	241	0.9	117.9	766	2.8	374.7	NT
NS5b	201,504	31,921	0.16	29	4.6	39	0.1	5.6	898	2.8	129.2	NT
BCC5a	162,406	401,500	2.47	10	24.7	9	0.0	0.6	3,122	0.8	192.2	NT
BCC5b	168,053	319,302	1.90	10	19.0	9	0.0	0.5	2,958	0.9	176.0	NT
MKL-1a	139,582	361,783	2.59	10	25.9	42,849	11.8	3069.8	2	0.0	0.1	NT
MCC13	140,958	216,455	1.54	10	15.4	9	0.0	0.6	0	0.0	0.0	NT
MCC26	177,471	130,675	0.74	10	7.4	23	0.0	1.3	0	0.0	0.0	NT
MS-1	107,475	448,106	4.17	10	41.7	57,523	12.8	5352.2	0	0.0	0.0	NT
MKL-1b	152,483	434,595	2.85	10	28.5	35,912	8.3	2355.1	0	0.0	0.0	NT
UIS0	199,572	150,539	0.75	10	7.5	37	0.0	1.9	0	0.0	0.0	NT
MKL-1c	138,724	197,841	1.43	10	14.3	19,503	9.9	1405.9	0	0.0	0.0	NT
MKL-2	168,396	190,566	1.13	10	11.3	18,734	9.8	1112.5	0	0.0	0.0	NT

Table S3. Total and specific miRNA concentrations in clinical samples. Total miRNA and specific miR-205 and miR-375 concentrations were derived for all samples. Relative miR-375 expression levels, derived from real-time RT-PCR measurements, indicate relative fold expression in each sample over a reference value (arbitrarily set at 1) from an NS sample. NT denotes not tested.

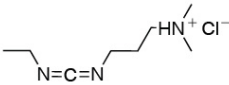
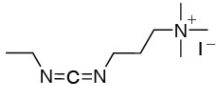
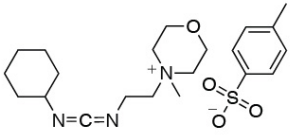
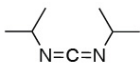
Carbodiimide derivative	Reaction time (h)	Reaction temperature (°C)	Optimal reaction pH
 Ethyl-3-(3-dimethylaminopropyl)carbodiimide hydrochloride (EDC-HCl)	28	25	8.0
	7	50	8.0
 Ethyl-3-(3-dimethylaminopropyl)carbodiimide methiodide (EDC-Mel)	12	25	8.0
	3	50	7.5
 N-Cyclohexyl-N'-(2-morpholinoethyl)carbodiimide metho- <i>p</i> -toluenesulfonate (CMC)	10	50	7.5
 N,N'-Diisopropylcarbodiimide (DIC)	24	50	8.0

Table S4. Optimized condensation reaction conditions using different carbodiimide derivatives.

Four different carbodiimide derivatives (0.1 M) were tested to identify optimal reaction conditions for phosphate activation while minimizing hydrolysis in 1-methylimidazole buffer (0.1 M 1-methylimidazole-HCl, pH 8.0, 0.3 M NaCl). Despite the shorter reaction time for EDC-Mel, we selected EDC-HCl to avoid overcrosslinking, which would decrease access of antibody-based signal amplification reagents to the target-RNA-bound probe-conjugated hapten.

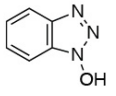
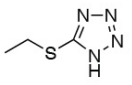
Heterocyclic derivative	Reaction time (h)	Reaction temperature (°C)	Optimal reaction pH
 2-Methylimidazole pKa ~ 7.8	14	50	8.0
 Imidazole pKa ~ 7.0	11	50	7.5 - 8.0
 1-Hydroxy-benzotriazole pKa ~ 5.0	4	50	8.0 - 8.5
 5-Ethylthio-1H-tetrazole pKa ~ 4.3	3	50	8.0
 2-Chloroimidazole pKa ~ 2.0	15	50	8.0

Table S5. Optimized condensation reaction conditions using different heterocyclic derivatives and EDC-HCl. Five different heterocyclic derivatives (0.1 M) combined with EDC-HCl (0.1 M) in 1-methylimidazole buffer were tested to identify optimal reaction conditions for minimizing hydrolysis through intermediate formation. For miRNA FISH experiments, we selected EDC-HCl and 5-ETT in 1-methylimidazole buffer.

A

	Probe	Length (nt)	Antisense probe	T _m (°C)
hsa-miR-205	LNA	22	5' CaGaCTCCGGtGGAatGaaGGa	70.7
	DNA	22	5' CAGACTCCGGTGGAAATGAAGGA	41.3
	LNA	14	5' GGTGGAAtgaAgga	61.6
	LNA	14	5' GGTGGAAtGaAggA	58.5
	DNA	14	5' GGTGGAATGAAGGA	33.1
hsa-miR-375	LNA	22	5' tCaCGCGAgcCGAAcgAaCaAa	73.0
	DNA	22	5' TCACGCGAGCCGAACGAACAAA	38.2
	LNA	15	5' agcCGaaCGaAcaaA	75.9
	LNA	15	5' AGCCGaaCGaAcaaA	62.1
	LNA	15	5' aGCCGaaCGaACaAa	53.8
	LNA	15	5' aGCCGaaCgAacAAa	63.3
	DNA	15	5' AGCCGAACGAACAAA	30.3

B

	Probe	Length (nt)	Antisense probe	T _m (°C)
hsa-rRNA	LNA1	17	5' CTttTcTgGgGTcTGaT	83.5
	LNA2	19	5' CAGcGCcATcCATTTtCAG	78.5
	LNA3	18	5' CATCTcTcAGGAcCgAcT	77.3
	LNA4	17	5' GGTtCctCtCGtACTgA	78.2

Table S6. miRNA and rRNA probe sequences and melting temperatures of duplexes with target RNA. (A) Several probes were designed to detect miR-205 (sense RNA sequence: 5'UCCUUAUCCACCGGAGUCUG) and miR-375 (sense RNA sequence: 5'UUUGUUCGUUCGGCUCGCGUGA); LNA residues are indicated in lowercase letters. Probe sequences that were used in the current study are highlighted in blue. (B) Four probes were designed to detect human 28S rRNA. The sense RNA sequences for LNA1, LNA2, LNA3 and LNA4 were 5'AUCAGACCCCAGAAAAG, 5'CUGAAA AUGGAUGGCGCUG, 5'AGUCGGUCCUGAGAGAUG and 5'UCAGUACGAGAGGAACC, respectively. These LNA-modified DNA probes also target mouse 28S rRNA. These probes were synthesized on 3'-amino-modifier C7 CPG (500 Å) solid glass support, deprotected, and conjugated to ATTO-647N-NHS ester. Melting temperatures were measured using 50% formamide, 1 M NaCl, and 50 mM phosphate (pH 7.0), and probe concentrations were 1.5 μM. Based on melting temperatures of the probes highlighted in blue, we chose a hybridization temperature slightly below at 55 °C for miRNA FISH experiments.

Sample name	miR-375 (mean intensity)	sum of pixels*	exposure (ms)	miR-205 (mean intensity)	sum of pixels*	exposure (ms)	rRNA (mean intensity)	sum of pixels*	exposure (ms)	miR-375 (normalized)#	miR-205 (normalized)#
MCC1	2207	78835	50	1090	1724	100	1196	72829	250	2.00	0.02
MCC2	2170	12005877	50	2017	539306	100	4085	12147745	250	0.53	0.02
MCC3	5411	123320	50	1215	12024	100	3272	123299	250	1.65	0.04
MCC4	2587	132879	50	1358	1921	100	2471	131663	250	1.06	0.01
MCC5	2215	131862	50	1426	9376	100	2009	130468	250	1.11	0.05
MCC6	2379	156358	50	1590	6079	100	2355	157611	250	1.00	0.03
MCC7	6556	11402977	50	1819	1751522	100	2571	11213780	250	2.59	0.11
MCC8	3270	10097631	50	1450	634629	100	3574	10097360	250	0.91	0.03
MCC9	1924	13851031	50	1889	156289	100	2591	11439599	250	0.90	0.01
MCC10	2538	72267	50	1379	3478	100	5431	71732	250	0.47	0.01
MCC11	2134	14805085	50	1627	557850	100	2640	14805779	250	0.81	0.02
MCC12	1802	12550860	50	1544	253568	100	4211	12550930	250	0.43	0.01
MCC13	2160	9513945	50	1443	508613	100	3099	10298898	250	0.64	0.02
BBC1	21	16	50	1967	59684	100	1889	68082	250	0.00	0.91
BBC2	33	1347	50	1642	13678440	100	1616	14872308	250	0.00	0.93
BBC3	12	22	50	1099	79182	100	832	99121	250	0.00	1.06
BBC4	1040	865	50	1755	69873	100	1641	72460	250	0.01	1.03
BBC5	1162	306310	50	1387	10758779	100	755	8360325	250	0.06	2.36

* sum of pixels above defined threshold, encompassing interval from 1,000 to 10,000 pixel intensities

$(\text{mean intensity of miRNA} \times \text{sum of pixels}) / (\text{mean intensity of rRNA} \times \text{sum of pixels})$

Table S7. miRNA signal normalization and establishment of cut-off values to enable tumor differential diagnosis. Mean signal intensities for miR-375, miR-205, and rRNA and the sum of pixels (encompassing the interval from 1,000 to 10,000 pixel intensities representing specific RNA signal and excluding background signal) for five BCC and thirteen MCC were recorded. Exposure times for miR-375, miR-205, and rRNA were 50, 100, and 250 ms, respectively.

Target	Fluorescent dye	Ex.	Em.	QY	Filter
Nuclei/DNA	DAPI	358 nm	460 nm	0.60	310 nm - 390 nm (Ex.) 430 nm - 480 nm (Em.)
miR-375	ATTO 488	500 nm	523 nm	0.80	475 nm - 505 nm (Ex.) 505 nm - 550 nm (Em.)
miR-205	ATTO 532	532 nm	553 nm	0.90	535 nm - 575 nm (Ex.) 570 nm - 650 nm (Em.)
rRNA	ATTO 647N	644 nm	669 nm	0.65	620 nm - 650 nm (Ex.) 660 nm - 705 nm (Em.)

Table S8. Fluorescent dyes and their properties, and filters for fluorescent imaging. Specific fluorescent dyes were used to identify DNA (nuclei) and RNA (miR-375, miR-205 and rRNA) targets in our study. Excitation (Ex.) and emission (Em.) wavelengths and the quantum yield (QY) of each dye, and the excitation and emission filters for the Sedat Quad filter set are indicated.